The Astronomical Journal, 128:1455–1464, 2004 September

EFFICIENT ORBIT INTEGRATION BY THE ORBITAL LONGITUDE METHOD USING ANTIFOCAL ANOMALY

Toshio Fukushima
National Astronomical Observatory, 2-21-1 Osawa, Mitaka, Tokyo 181-8588, Japan; Toshio.Fukushima@nao.ac.jp
Received 2004 May 18; accepted 2004 June 3

ABSTRACT

Adopting the antifocal anomaly as the basis of a new orbital longitude, we obtain a variation on the true-longitude method to numerically integrate perturbed Keplerian orbits. Although the new method is applicable to elliptical orbits only, it achieves a larger stability region and gives significantly smaller integration errors than the original method when the perturbations are small and the eccentricity is not too large.

Key words: celestial mechanics — methods: *n*-body simulations

1. INTRODUCTION

Recently we succeeded in significantly reducing the accumulation of round-off errors in the orbital longitude method for numerically integrating perturbed Keplerian orbits (Fukushima 2004d).[1] This is accomplished by taking the modulus of the angle variables with 2π at each integration step if necessary. The improved method, which we call the true-longitude method for short, has better cost performance than the standard method to integrate the motion in rectangular coordinates and its variations—the methods of manifold correction (Fukushima 2003a, 2003b, 2003c, 2004a, 2004b, 2004c).[2] The true-longitude method is a sort of variable transformation method using a set of one fast and five slow variables. The fast variable is a true orbital longitude measured from a longitude origin solely determined by the orbital angular momentum and the initial position vector. The slow variables are the deviations of five quantities from their initial values. Here the five quantities consist of the three rectangular components of the orbital angular momentum and the two independent components of the Laplace integral vector on the orbital plane.

Numerical experiments showed that the true-longitude method has better cost performance than our existing methods of manifold correction (see Paper VII). For Keplerian orbits, the method produces only minute periodic errors for a usefully long integration time if a sufficiently high order integrator is used with a sufficiently small step size. This owes greatly to the fact that our formulation becomes a one-dimensional problem for Keplerian orbits, since the five slow variables remain zero in that case. See Figure 1, showing the integration errors of the fast variable, which essentially reduces to the true anomaly for Keplerian orbits. The errors are suppressed at the level of 10^{-11} radians for more than a million orbital periods. (See also Fig. 2, for the periodic nature of the errors.) This is the case of a moderate eccentricity, $e = 0.1$. In performing the integrations, we used the 13th-order implicit Adams method in PECE mode (predict, evaluate, correct, evaluate) as the integrator, fixed the step size at 1/64 the orbital period, and prepared the starting tables with Gragg's extrapolation method. In plotting these figures, we measured the errors by comparing with reference solutions obtained using the same integrator and the same model parameters but half the step size. The magnitude of the observed periodic errors reduces to the level of the machine epsilon if we use a higher order integrator[3] or a smaller step size. When perturbations exist, on the other hand, the errors first grow in proportion to the square root of time for a certain amount of time, the length of which depends on the magnitude of the perturbations (Figs. 8–12 below).

We confirmed that these good properties of the true-longitude method are independent of various aspects of the integration of perturbed orbits: the method of integration, the policy governing step-size control, the kind of perturbation, and the type of unperturbed orbit—whether elliptical, parabolic, or hyperbolic. On the other hand, the total cost of integration in the true-longitude method is almost the same as that of the standard method. As we learned in Paper VII and stressed above, these excellent characteristics are mainly due to the fact that the equations of motion in the true-longitude method reduce to one dimension when the perturbation vanishes, that of the true anomaly (see eq. [A22] in Appendix A).

However, this is not a property possessed by the true anomaly only. In general, there are other angles that can be used in place of the true anomaly.[4] Among them, we note the antifocal anomaly, the polar angle in a coordinate system that adopts as its coordinate origin not the primary but the secondary focus of the orbital ellipse (see Fig. 3 for a geometric definition and refer to Appendix A for a summary of its basic properties). Although useless for parabolic orbits, the antifocal anomaly has a better feature than the true anomaly for moderately eccentric and near-circular orbits. In fact, its expansion with respect to the mean anomaly begins from the second power of the eccentricity (see eq. [A23]). In other words, the antifocal anomaly increases more uniformly with respect to time than the true and other anomalies such as the eccentric one. Thus, it is to be expected that its numerical integration will lead to smaller errors for Keplerian orbits when the eccentricity is small. This is true, as can be seen in Figures 1 and 2, where both the results are after application of the round-off reduction we discovered in Paper VII. Of course, whether this works for perturbed orbits is a different issue to be investigated.

In this paper, we report that a variation of the true-longitude method based on the antifocal anomaly performs better than the original method for elliptical orbits if the perturbations are small and the nominal eccentricity is not too large. In the

[1] Hereafter Paper VII.
[2] Hereafter Papers I–VI, respectively.
[3] Of course, the order must be low enough to cause no numerical instabilities.
[4] Well-known examples are the eccentric and the mean anomalies. However, we experienced some technical difficulty in properly extending them to serve as the orbital longitude.

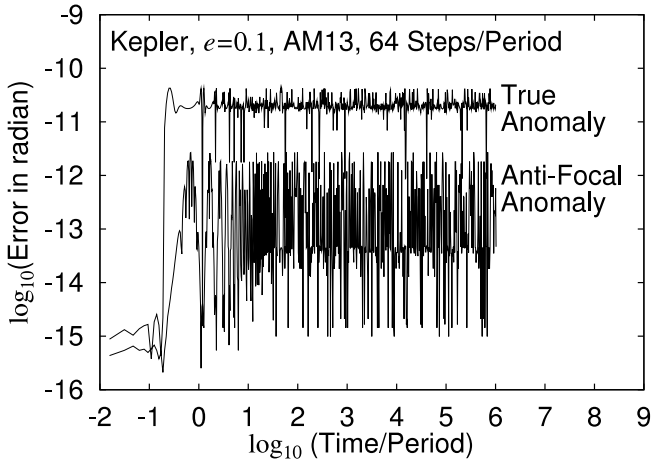

FIG. 1.—Numerical integration errors for the true and the antifocal anomalies. The absolute errors for a Keplerian orbit with $e = 0.1$ are plotted on a log-log scale. The adopted integrator is the 13th-order implicit Adams method in PECE mode, the step size was fixed as 1/64 the orbital period, the starting tables were prepared with Gragg's extrapolation method, and the errors were measured by comparing with reference solutions obtained using the same integrator and the same model parameters but with half the step size. Both results include the round-off reduction by taking the modulus of the anomaly with 2π at each integration step when necessary.

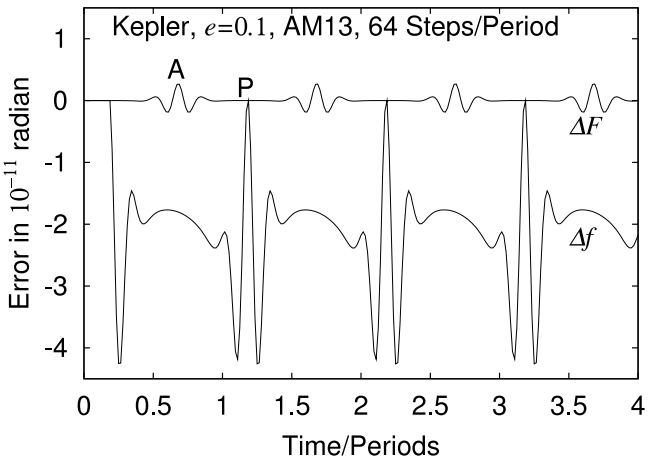

FIG. 2.—Close-up of the integration errors for the true and antifocal anomalies, plotted on a linear-linear scale for the first few orbital periods. The periodic error in the true anomaly Δf has a peak at pericenter passage (P) while that in the antifocal anomaly ΔF has a peak at apocenter (A). Note that Δf is too small to be visible in this scale until the first pericenter passage. Although we show the results for the first four periods, we have confirmed that the same situation continues up to more than 1 million orbital periods.

following, we describe the modification of the true-longitude method in § 2 and present a numerical comparison with the original true-longitude method in § 3.

2. ORBITAL LONGITUDE METHOD USING ANTIFOCAL ANOMALY

Let us construct the orbital longitude method using the antifocal anomaly in place of the true anomaly. To do this, however, we must backtrack to an earlier stage, Paper V, where we invented a simplification of the linear transformation method that we developed in Paper IV.

The first simplification of the linear transformation method given in Paper V uses a set of nine variables per celestial body, $(\boldsymbol{x}, \Delta\boldsymbol{L}, \Delta\boldsymbol{P})$. Here $\boldsymbol{x}$ is the position vector referred to the primary focus, $\Delta\boldsymbol{L}$ is the deviation of the orbital angular momentum vector from its initial value, and $\Delta\boldsymbol{P}$ is similarly the deviation of the Laplace integral vector. Appendix B contains a summary of the simplified method using this set.

Below, we describe the details of the construction in two stages: (1) the introduction of the antifocal position vector and (2) its three-step transformation into the antifocal orbital longitude.

2.1. *Antifocal Position Vector*

By changing the coordinate origin from the primary to the secondary focus, we introduce various antifocal quantities: (1) $\boldsymbol{X}$, the antifocal position vector; (2) $\boldsymbol{V} \equiv d\boldsymbol{X}/dt$, the antifocal velocity vector; (3) $R \equiv |\boldsymbol{X}|$, the antifocal radius; and (4) $\boldsymbol{N} \equiv \boldsymbol{X}/R$, the antifocal unit position vector. See Figure 3 for geometric definitions of $\boldsymbol{X}$ and R.

The basic relation[5] between these antifocal quantities and those referred to the primary focus is

$$\boldsymbol{X} = \boldsymbol{x} + \boldsymbol{S}. \tag{1}$$

[5] This holds because (1) the Laplace vector is in the direction from the primary focus to the pericenter and, therefore, is also parallel to the direction from the secondary to the primary focus, and (2) the distance between the two foci is $2ae$, where a is the semimajor axis and e is the orbital eccentricity.

Here

$$\boldsymbol{S} = \alpha\boldsymbol{P} \tag{2}$$

is the separation vector between the two foci, and

$$\alpha \equiv \frac{2a}{\mu} = \frac{2L^2}{\mu^2 - P^2} \tag{3}$$

is a parameter related to the semimajor axis a and the gravitational constant $\mu \equiv GM$. In the above rewriting,[6] L and P

[6] The rewriting of α is derived from the condition $\alpha P = 2ae$, noting the expressions of L and P in terms of the Keplerian elements as $L = [\mu a(1 - e^2)]^{1/2}$ and $P = \mu e$.

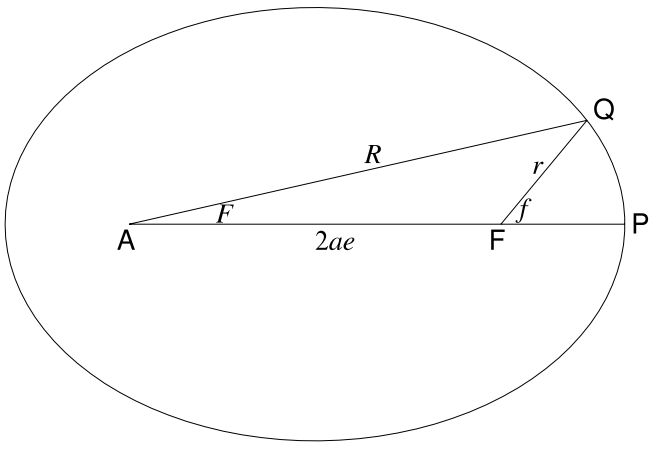

FIG. 3.—Schematic diagram illustrating the antifocal anomaly and the antifocal radius. Shown are the primary focus (F), the secondary focus (A), the pericenter (P), and a point on the ellipse (Q). Then the antifocal radius R and the antifocal anomaly F are geometrically defined as $R \equiv \mathrm{AQ}$ and $F \equiv \angle\mathrm{QAP}$. Similarly, the radius r and the true anomaly f are defined as $r \equiv \mathrm{FQ}$ and $f \equiv \angle\mathrm{QFP}$. The separation between the two foci is $2ae$, where a and e are the semimajor axis and the eccentricity of the ellipse, respectively. The eccentricity of the ellipse illustrated here is 0.6. The sum of R and r is constant, $R + r = 2a$. The antifocal position vector $\boldsymbol{X}$ and the usual position vector $\boldsymbol{x}$ are defined as $\boldsymbol{X} \equiv \overrightarrow{\mathrm{AQ}}$ and $\boldsymbol{x} \equiv \overrightarrow{\mathrm{FQ}}$, while the focus separation vector $\boldsymbol{S}$ is defined as $\boldsymbol{S} \equiv \overrightarrow{\mathrm{AF}}$.

are the magnitudes of the orbital angular momentum vector $\boldsymbol{L}$ and of the Laplace integral vector $\boldsymbol{P}$, respectively.

The corresponding relation for the velocity becomes

$$\boldsymbol{V} = \boldsymbol{v} + \boldsymbol{U}, \tag{4}$$

where

$$\boldsymbol{U} \equiv \frac{d\boldsymbol{S}}{dt} = \left(\frac{\alpha \boldsymbol{L}\cdot\boldsymbol{M} + \alpha^2 \boldsymbol{P}\cdot\boldsymbol{Q}}{L^2}\right)\boldsymbol{P} + \alpha \boldsymbol{Q} \tag{5}$$

is a quantity that vanishes for Keplerian orbits and

$$\boldsymbol{M} \equiv \frac{d\boldsymbol{L}}{dt}, \quad \boldsymbol{Q} \equiv \frac{d\boldsymbol{P}}{dt}. \tag{6}$$

From Appendix A, we have that the antifocal radius is expressed in terms of $\boldsymbol{N}$, $\boldsymbol{L}$, and $\boldsymbol{P}$ as

$$R = \frac{L^2}{\mu - \boldsymbol{P}\cdot\boldsymbol{N}}. \tag{7}$$

This is similar to equation (A4) in Appendix A, its counterpart for r, the radius referred to the primary focus. From the defining property of the ellipse, we know that the sum of the two radii is constant. Then r is obtained from R as

$$r = \mu\alpha - R. \tag{8}$$

Using these two expressions for R and r, as well as equations (1) and (3), we rewrite[7] the expression for the velocity vector referred to the primary focus, equation (B5) in Appendix B, as

$$\boldsymbol{v} = \frac{R\boldsymbol{L}\times(\mu\boldsymbol{N} - \boldsymbol{P})}{rL^2}. \tag{9}$$

Finally, the equation of motion for $\boldsymbol{X}$ becomes simply

$$\frac{d\boldsymbol{X}}{dt} = \boldsymbol{V} = \boldsymbol{v} + \boldsymbol{U}, \tag{10}$$

where the expressions for $\boldsymbol{v}$ and $\boldsymbol{U}$ are as given above.

Then we are ready to obtain a variant of the first simplification of the linear transformation method provided in Paper V using the set ($\boldsymbol{X}$, $\Delta\boldsymbol{L}$, $\Delta\boldsymbol{P}$). The resulting method is summarized in Appendix C.

2.2. *Antifocal Orbital Longitude*

Once the simplification of the linear transformation method using the antifocal position vector $\boldsymbol{X}$ is established as in Appendix C, the remaining tasks to obtain the orbital longitude method using the antifocal anomaly are straightforward, as we did for the true-longitude method in Papers V and VI.

In particular, the procedure consists of the following three steps: We first replace the antifocal position vector $\boldsymbol{X}$ by its unit vector $\boldsymbol{N}$. The resulting method is a variation of the simplified linear transformation method using another set of nine antifocal variables, ($\boldsymbol{N}$, $\Delta\boldsymbol{L}$, $\Delta\boldsymbol{P}$). Second, we introduce the coordinate triad ($\boldsymbol{e}_A$, $\boldsymbol{e}_B$, $\boldsymbol{e}_C$) referred to the orbital plane as we did in Paper VI. As a result, we reduce the number of variables to seven, (N_A, N_B, $\Delta\boldsymbol{L}$, ΔP_A, ΔP_B). Finally, we express N_A and N_B in terms of the antifocal longitude, w, as

$$N_A = \cos w, \quad N_B = \sin w. \tag{11}$$

Here w is the same as the antifocal anomaly but is measured from a longitude origin defined as the direction of $\boldsymbol{e}_A$. The method finally obtained is the orbital longitude method based on the antifocal orbital longitude. It uses a new set of six variables, (w, $\Delta\boldsymbol{L}$, ΔP_A, ΔP_B).

The core part of the new method is the equation of motion of the angle w:

$$\frac{dw}{dt} = \Omega_W + \Omega_S + \Omega_F. \tag{12}$$

Here

$$\Omega_W \equiv L/(rR) \tag{13}$$

is the angular velocity of the orbital motion around the secondary focus. This has the same form as in the Keplerian case, equation (A26) in Appendix A. Next,

$$\Omega_S \equiv \frac{(\boldsymbol{N}\times\boldsymbol{U})\cdot\boldsymbol{e}_C}{R} \tag{14}$$

is the angular velocity of the rotation associated with the perturbed motion of the focus separation vector, $\boldsymbol{S}$. Finally, Ω_F is the angular velocity of the frame rotation due to perturbation of the orbital angular momentum vector, which was discussed extensively in Paper VI.

Originally, equation (14) is derived[8] from the equation of motion for $\boldsymbol{N}$,

$$\frac{d\boldsymbol{N}}{dt} = \boldsymbol{\Omega}_N \times \boldsymbol{N}, \tag{15}$$

where $\boldsymbol{\Omega}_N$ is defined[9] as

$$\boldsymbol{\Omega}_N \equiv \frac{\boldsymbol{N}\times\boldsymbol{V}}{R}. \tag{16}$$

Using equations (7), (11), and (12), we rewrite the above definition[10] as

$$\boldsymbol{\Omega}_N = \frac{\boldsymbol{L}}{rR} + \frac{\boldsymbol{N}\times\boldsymbol{U}}{R}, \tag{17}$$

---

[7] In detail,

$$\boldsymbol{v} = \frac{\boldsymbol{L}\times(\mu\boldsymbol{n} + \boldsymbol{P})}{L^2} = \frac{\boldsymbol{L}\times(\mu\boldsymbol{x} + r\boldsymbol{P})}{rL^2} = \frac{\boldsymbol{L}\times[\mu(\boldsymbol{X} - \boldsymbol{S}) + r\boldsymbol{P}]}{rL^2}$$
$$= \frac{\boldsymbol{L}\times[\mu\boldsymbol{X} - (\mu\alpha - r)\boldsymbol{P}]}{rL^2} = \frac{\boldsymbol{L}\times(\mu R\boldsymbol{N} - R\boldsymbol{P})}{rL^2} = \frac{R\boldsymbol{L}\times(\mu\boldsymbol{N} - \boldsymbol{P})}{rL^2}.$$

[8] This form for the equation of motion of a unit vector is of a general nature, since the identity $(d\boldsymbol{N}/dt)\cdot\boldsymbol{N} = 0$ always holds. This is derived from the differentiation of the normalization condition, $\boldsymbol{N}^2 = 1$.

[9] This definition is derived from the expression

$$\boldsymbol{V} = \frac{d\boldsymbol{X}}{dt} = \frac{d\,R\boldsymbol{N}}{dt} = \frac{dR}{dt}\boldsymbol{N} + R\frac{d\boldsymbol{N}}{dt} = \frac{dR}{dt}\boldsymbol{N} + (R\boldsymbol{\Omega}_N \times \boldsymbol{N}),$$

by taking the vector products of both sides with $\boldsymbol{N}$.

[10] The details of the rewriting for the part in v are as follows:

$$\frac{\boldsymbol{N}\times v}{R} = \frac{\boldsymbol{N}}{R}\times\frac{R\boldsymbol{L}\times(\mu\boldsymbol{N} - \boldsymbol{P})}{rL^2} = \frac{\boldsymbol{N}\times[\boldsymbol{L}\times(\mu\boldsymbol{N} - \boldsymbol{P})]}{rL^2}$$
$$= \frac{[\boldsymbol{N}\cdot(\mu\boldsymbol{N} - \boldsymbol{P})]\boldsymbol{L}}{rL^2} = \frac{(\mu - \boldsymbol{P}\cdot\boldsymbol{N})\boldsymbol{L}}{rL^2} = \frac{\boldsymbol{L}}{rR},$$

where we have used the identities $\boldsymbol{N}^2 = 1$ and $\boldsymbol{N}\cdot\boldsymbol{L} = 0$.

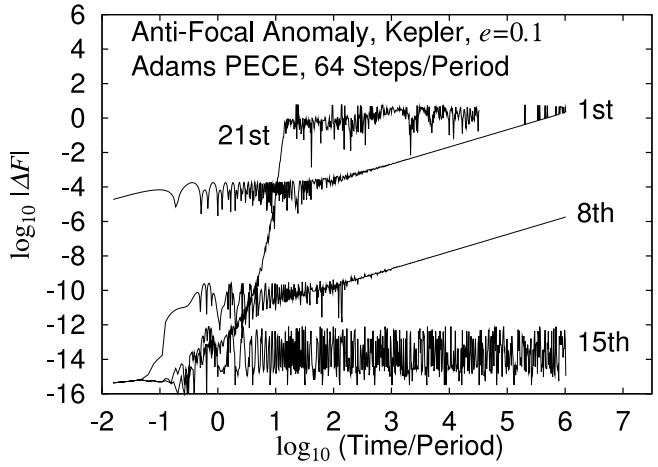

FIG. 4.—Order dependence of the numerical integration errors for the antifocal anomaly, plotted for different orders of the implicit Adams method. Here the step size and the eccentricity are fixed at 1/64 the orbital period and $e = 0.1$, respectively. If the order is as low as 1 or 8, the errors remain periodic for some integration period and then grow linearly with respect to time. For the moderately high order of 15, the errors remain finite. On the other hand, for the too-high order of 21, the errors grow exponentially.

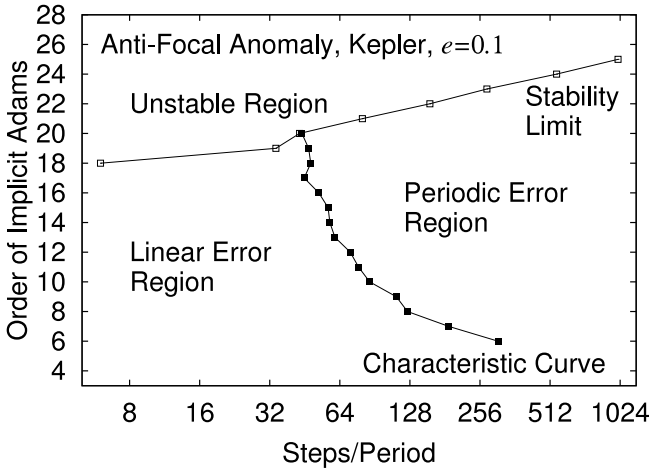

FIG. 5.—Diagram of order vs. step size for the antifocal anomaly F. The plane (for the implicit Adams method in PECE mode) separates into three regions: an unstable region, a region of purely periodic errors, and a region of linearly growing error over the long run.

which leads to the final expressions for Ω_W and Ω_S.[11] The addition of Ω_F is due to the introduction of the coordinate triad, as explained in Paper VI.

The whole procedure for the new orbital longitude method is summarized in Appendix D.

3. NUMERICAL EXPERIMENTS

Let us compare the performance of the new orbital longitude method using the antifocal orbital longitude with that of the original one, using the true orbital longitude.

We begin with the Keplerian orbits. In these cases, the problem is reduced to one dimension, namely, the integration of the true anomaly f and that of the antifocal anomaly F. From Appendix A, their equations of motion are

$$\frac{df}{dt} = \nu(1 + e\cos f)^2,$$
$$\frac{dF}{dt} = \nu\left(\frac{1 - 2e\cos F + e^2\cos^2 F}{1 - 2e\cos F + e^2}\right), \qquad (18)$$

where $\nu = n/(1 - e^2)^{3/2}$ is a constant of time computed from the mean motion n and the eccentricity e.

If we integrate these equations with a given integrator, we face three kinds of error growth with respect to time: (1) the case showing exponential or faster growth, (2) the case of linear growth, and (3) the case of no growth, which we saw in Figure 1 already. Figure 4 shows the integration errors as functions of time for the antifocal anomaly in the case of $e = 0.1$. Here the step size was fixed at 1/64 the orbital period, while the order of the implicit Adams method in PECE mode was varied from 1 to 21. In the figure, use of an extremely high order such as the 21st leads to the first case, usually described as numerical instability. The second case occurs for low orders such as the first and the eighth, which first show only periodic errors but exhibit linear growth in the long run. The last case corresponds to a moderately high order such as the 15th, which produces only the periodic errors.

By conducting test integrations for vast combinations of the order and step size while fixing the eccentricity at $e = 0.1$, we prepared Figures 5 and 6, showing two-dimensional diagrams of the manner of error growth with respect to the order and step size for the antifocal and true anomalies, respectively. First we observe that the numerical integration of the antifocal anomaly is much more stable than that of the true anomaly. Compare the lines indicating the stability limit in the two graphs, which separate the unstable region and the other two. The cost of multistep methods such as the Adams method mainly depends not on the order but on the step size. On the other hand, their performance greatly depends on the order for a given step size. Thus the superiority in numerical stability means higher cost performance. For example, the difference in the available maximum order amounts to 4 or 5 for typical step sizes corresponding to the range of 32 to 128 steps per period. This means that we may expect a gain in precision of

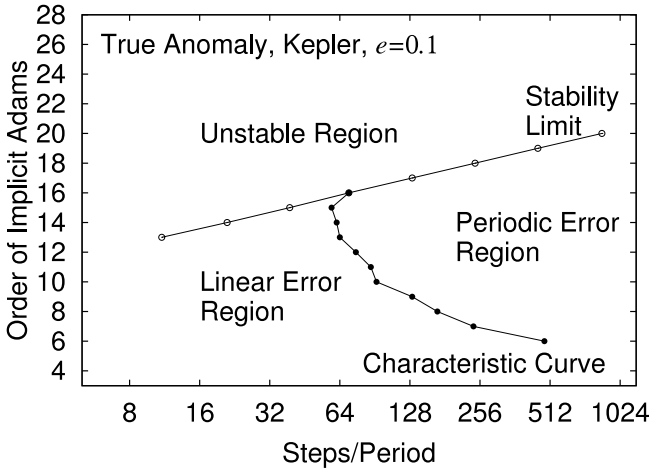

FIG. 6.—Same as Fig. 5, but for the true anomaly, f.

[11] The derivation is easy, since $\Omega_W = (rR)^{-1}\boldsymbol{L}\cdot\boldsymbol{e}_C$, $\Omega_S = (\boldsymbol{N}\times\boldsymbol{U}/R)\cdot\boldsymbol{e}_C$, and $\boldsymbol{e}_C \equiv \boldsymbol{L}/L$.

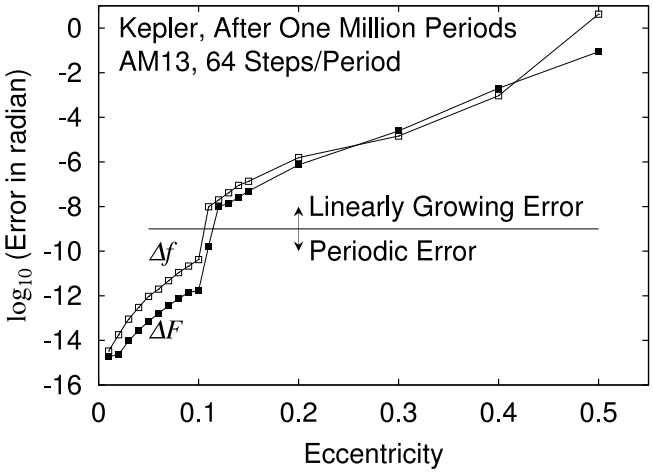

FIG. 7.—Eccentricity dependence of integration errors for the true and the antifocal anomalies. The diagram compares the errors in Keplerian orbits of different eccentricities after integration for 1 million orbital periods.

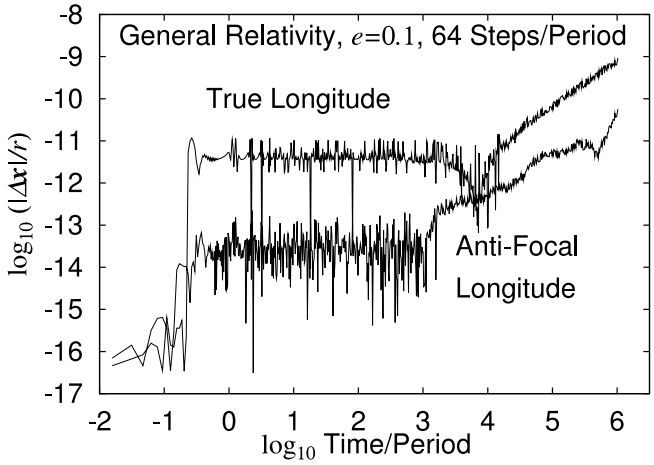

FIG. 8.—Effect of weak perturbations on the two orbital longitude methods. Compared are the errors for a planet under post-Newtonian perturbations of relative magnitude 10^{-8}, roughly the same as the Sun's perturbation acting on Earth. The orbit is of moderate nominal eccentricity and inclination, $e = 0.1$ and $I = 23^\circ$, respectively. The step size is 1/64 the nominal orbital period and the integrator is the implicit Adams method in PECE mode. The order of the integrator was chosen to be the highest that remained stable: 15 for the method using the true orbital longitude and 20 for that using the antifocal longitude.

around two to six digits.[12] On the other hand, the separation between the regions of linearly growing errors and of periodic errors is mostly the same (the lines denoted "characteristic curve" in the graphs).

We assume that the magnitude of the integration errors of these anomalies is in proportion to that of the nonlinear components of the angles themselves. From equations (A15) and (A16) in Appendix A, we can see that the nonlinear component of the antifocal anomaly is smaller than that of the true anomaly by a factor of $e/8$ when the eccentricity is sufficiently small. Then, even under the condition that the same-order integrator is used with the same step size, we also expect a gain in precision of the above factor or so by replacing the true anomaly with the antifocal anomaly. Figure 7 shows the eccentricity dependence of the integration errors in f and F, where the integrator and the step size are fixed as the 13th-order implicit Adams method in PECE mode and 1/64 the orbital period, respectively. There exists a critical value of eccentricity, $e = 0.10$ in this case. The integration errors for the orbits with eccentricity equal to or less than this critical value remain periodic for a usefully long integration time. Otherwise, the errors seem to be periodic for some initial duration, say, 1000 orbital periods or so, and then increase linearly with respect to time. The above expectation roughly holds in the regime of periodic errors where the order of the integrator used is sufficiently high and the adopted step size is sufficiently small.

Let us move on to the perturbed cases. Figure 8 shows the case of a weak perturbation, that of a post-Newtonian effect of relative magnitude 10^{-8}. This is the same order of magnitude as Earth feels from the general relativistic effect of the Sun. In this case, the orders of the integrator were set to the highest among those that led to no numerical instabilities. This is to examine the maximum cost performance, that is, to explore the highest precision for the same computational time. The resulting orders are 15 for the true-longitude method and 20 for the antifocal one. Imagine a cross section of Figures 5 and 6 along the lines of 64 steps per period. This large difference in the maximum available order of the integrator results a large difference in the integration errors, as well as in the manner of error growth. Therefore, the antifocal longitude method is much superior to the true-longitude method in the case of weak perturbations.

Unfortunately, the superiority of the antifocal longitude method diminishes when the perturbations become larger. Figure 9 shows such an example, the case of an artificial satellite under the J_2 perturbation of Earth. This time the semimajor axis of the orbit was taken to be as small as Earth's radius. This is an extreme case for a J_2-type perturbation. The maximum available orders are 15 for the true-longitude method and 17 for the antifocal one. In this case, the errors of the antifocal longitude method are significantly smaller than those of the true-longitude method for the first few thousand periods. However, this situation is reversed in the long run.

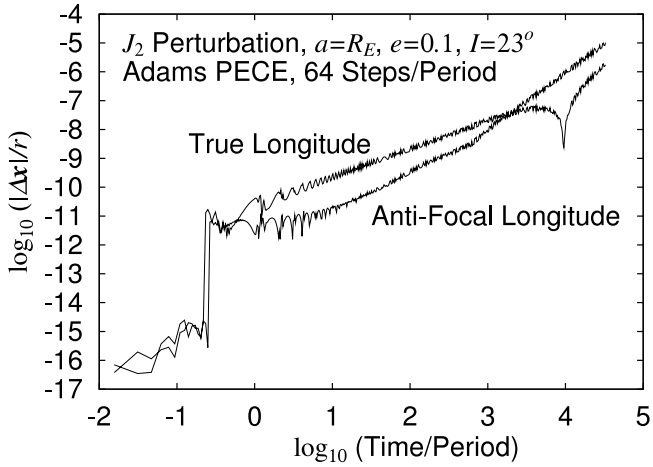

FIG. 9.—Same as Fig. 8, but for moderate perturbations. Shown are the errors for an Earth-grazing orbit of an artificial satellite under J_2 perturbation. The (highest stable) orders of the integrators are 15 for the method using the true orbital longitude and 17 for that using the antifocal longitude. The errors of the new method are smaller for the first few thousand periods, and then the situation reverses.

[12] In reality, however, the gain in precision is a few digits in most cases.

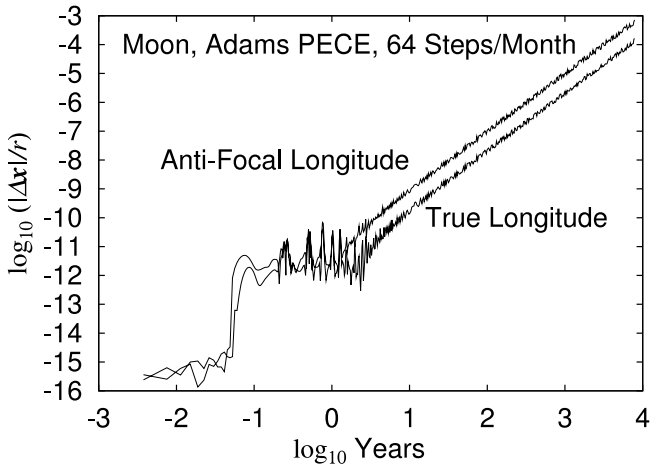

FIG. 10.—Same as Fig. 8, but for strong perturbations. Shown are the errors in the position of the Moon in the restricted three-body problem of the Sun, Earth, and the Moon, the so-called main problem of lunar theory. The step size is 1/64 the sidereal month. The (highest stable) orders of the integrators are 15 for the method using the true orbital longitude and 14 for that using the antifocal longitude. This time, the perturbation on the vector separating the foci is so strong that the new method is of lower stability than the original orbital longitude method, as reflected in the observed difference in performance.

In cases of strong perturbation, the inferiority of the antifocal longitude method is clear. See Figure 10, which illustrates the position errors of the Moon in the restricted three-body problem of the Sun, Earth, and the Moon, the so-called main problem of lunar theory. This time the maximum available orders are 15 for the true-longitude method and 14 for the antifocal method. Examining the variations of four angular velocities, Ω_W, Ω_S, $\Omega_C \equiv L/r^2$, and Ω_F, we learn that Ω_S oscillates so strongly[13] in this case that the integration of the antifocal orbital longitude is less stable than that of true orbital longitude. This difference in stability results in the observed difference in the magnitude of the integration errors.

Figure 11 depicts a comparison of integration errors in a complicated problem, the errors of Mercury in a simultaneous integration of the Sun and nine major planets. This is a case of moderate perturbations, as the J_2 perturbation. This time the maximum available orders are 15 for the true-longitude method and 18 for the antifocal one. At the outset, the superiority of the antifocal longitude method is obvious. However, the true-longitude method wins in the end.

Finally, let us examine the behavior of the new method in the region where round-off errors play the key role. Figure 12 shows a curve similar to that in Figure 11 but for the new method, fixing the step size at 0.70 days and using the 13th-order implicit Adams method in PECE mode. Comparing this with the similar graph for the true-longitude method, Figure 9 of Paper VII, we can see that the new method gives almost the same performance in the cases where round-off errors are dominant. Namely, the integration errors first grow in proportion to the square root of time for some period, 1000 years or so in this case, and then increase rapidly.

[13] It is well known that the eccentricity vector of the Moon liberates in such a wild fashion.

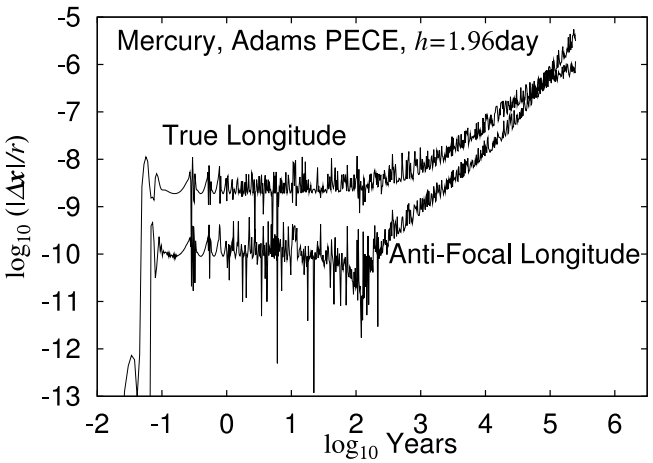

FIG. 11.—Effect of compound perturbations on the two orbital longitude methods. Shown are the errors of Mercury in a simultaneous integration of the Sun and nine major planets. The step size is 1.96 days, 1/64 the nominal orbital period of Mercury. The orders of the integrators are again the highest stable, 15 for the method using the true orbital longitude and 18 for that using the antifocal longitude.

4. CONCLUSION

Replacing the orbital longitude based on the true anomaly with one based on the antifocal anomaly, we have modified the improved orbital longitude method from Paper VII. The new method inherits all the good properties of the original method. However, the new method is no more universal; that is, it is applicable to elliptical orbits only. At the price of this demerit, the new method has better cost performance, namely, achieving higher precision results for the same computational time, than the original method in two cases: (1) when the perturbing acceleration is relatively small, and (2) when the strength of the perturbing acceleration is moderate and the integration time is short enough that the perturbations do not grow too much. In such cases, we recommend use of the new method for integrating perturbed Keplerian orbits numerically.

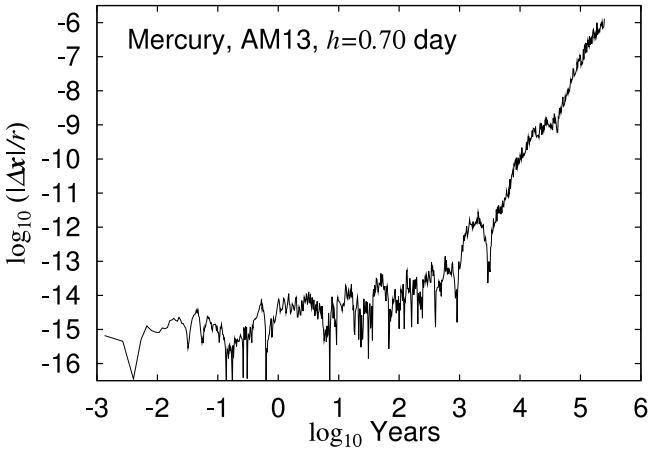

FIG. 12.—Same as Fig. 11, but for a step size of 0.70 days, 1/180 the nominal orbital period of Mercury. Combined with the adopted 13th-order integrator the step size is so small that round-off errors play the key role in the growth of overall integration error. We omit the graph for the true-longitude method, which is shown in Fig. 8 of Paper VII, since it is almost the same as that for the new method illustrated here.

APPENDIX A

ANTIFOCAL ANOMALY

Here we summarize the properties of the antifocal anomaly, F. In particular, the main target is the derivation of its equation of motion, used in the main text.

First of all, let us introduce a radius associated with the antifocal anomaly. We name it the antifocal radius. The pair of the antifocal radius R and the antifocal anomaly F are the polar coordinates of a point Q on an elliptical orbit in a coordinate system in which the coordinate origin is not the primary focus F but the secondary one, A, and the longitude origin is the pericenter, P, as usual (see Fig. 3). Then this polar angle F can be said to be an anomaly since it takes the value 0 at the pericenter and π at the apocenter. Let us denote the two-dimensional rectangular coordinates associated with the antifocal polar coordinates as (X, Y).

From the above definition, the rectangular coordinates of Q referred to the primary focus, (x, y), can be expressed in four ways: in terms of (1) the (true) radius r and the true anomaly f, (2) the semimajor axis a and the eccentric anomaly E, (3) the antifocal radius R and the antifocal anomaly F, and (4) the antifocal rectangular coordinates X and Y, respectively, as

$$x = r\cos f = a(\cos E - e) = R\cos F - 2ae = X - 2ae, \tag{A1}$$

$$y = r\sin f = a\sqrt{1-e^2}\sin E = R\sin F = Y, \tag{A2}$$

where e is the orbital eccentricity. From these, it is easily shown that R has an expression

$$R = \sqrt{X^2+Y^2} = a(1+e\cos E) = \frac{a(1-e^2)}{1-e\cos F}, \tag{A3}$$

which is similar to that for r,

$$r = \sqrt{x^2+y^2} = a(1-e\cos E) = \frac{a(1-e^2)}{1+e\cos f}. \tag{A4}$$

As a by-product, we prove the important property that the sum of R and r is constant,[14]

$$R + r = 2a. \tag{A5}$$

As a consequence, we obtain an expression for r in terms of F as

$$r = \frac{a(1-2e\cos F + e^2)}{1-e\cos F}, \tag{A6}$$

as well as its counterpart,

$$R = \frac{a(1+2e\cos f + e^2)}{1+e\cos f}. \tag{A7}$$

Another by-product is the anomaly-anomaly relation

$$(1+e\cos E)(1-e\cos F) = (1-e\cos E)(1+e\cos f) = 1-e^2. \tag{A8}$$

Using the tangent half-angle formulae, we obtain its more popular variation as

$$\sqrt{\frac{1+e}{1-e}}\tan\left(\frac{F}{2}\right) = \tan\left(\frac{E}{2}\right) = \sqrt{\frac{1-e}{1+e}}\tan\left(\frac{f}{2}\right). \tag{A9}$$

Unfortunately, these expressions are indefinite at the apocenter and, therefore, are insuficient from a practical point of view. Thus, we rewrite them in an effective form as

$$\begin{aligned} f &= F + 2\tan^{-1}\left(\frac{e\sin F}{1-e\cos F}\right) \\ &= E + 2\tan^{-1}\left[\frac{e^*\sin E}{(1-e)(1-e^*\cos E)}\right], \end{aligned} \tag{A10}$$

$$\begin{aligned} F &= f - 2\tan^{-1}\left(\frac{e\sin f}{1+e\cos f}\right) \\ &= E - 2\tan^{-1}\left[\frac{e^*\sin E}{(1+e)(1+e^*\cos E)}\right], \end{aligned} \tag{A11}$$

$$\begin{aligned} E &= F + 2\tan^{-1}\left[\frac{e^*\sin F}{(1-e)(1-e^*\cos F)}\right] \\ &= f - 2\tan^{-1}\left[\frac{e^*\sin f}{(1+e)(1+e^*\cos f)}\right], \end{aligned} \tag{A12}$$

where

$$e^* \equiv \frac{2e}{(\sqrt{1-e}+\sqrt{1+e})^2} \sim \frac{e}{2} + O(e^3). \tag{A13}$$

These are useful in obtaining f or F as a function of time or of the mean anomaly, M. This is done by way of E, which is determined by solving the Kepler equation

$$E - e\sin E = M. \tag{A14}$$

As a result, we obtain their expansions in M as follows:

$$f \sim M + 2e\sin M + \frac{5e^2}{4}\sin 2M + O(e^3), \tag{A15}$$

$$F \sim M + \frac{e^2}{4}\sin 2M + O(e^3). \tag{A16}$$

Thus the magnitudes of the nonlinear parts[15] of f and F are different roughly by a factor of $e/8$ when e is small.

Next, by differentiating the expressions for the rectangular coordinates with respect to time, we obtain the velocity components as

$$\begin{aligned} \frac{dx}{dt} &= \frac{dr}{dt}\cos f - r\sin f\left(\frac{df}{dt}\right) = -a\sin E\left(\frac{dE}{dt}\right) \\ &= \frac{dR}{dt}\cos F - R\sin F\left(\frac{dF}{dt}\right) = \frac{dX}{dt}, \end{aligned} \tag{A17}$$

[14] Rather, an ellipse is geometrically defined as the loci of a point satisfying this property.

[15] That of f is known as the equation of center.

$$\frac{dy}{dt} = \frac{dr}{dt}\sin f + r\cos f\left(\frac{df}{dt}\right) = a\sqrt{1-e^2}\cos E\left(\frac{dE}{dt}\right)$$
$$= \frac{dR}{dt}\sin F + R\cos F\left(\frac{dF}{dt}\right) = \frac{dY}{dt}, \tag{A18}$$

where we used the facts that a and e are constants of time. From these, we obtain the time derivatives of f and F in terms of that of E as

$$r^2\frac{df}{dt} = x\frac{dy}{dt} - y\frac{dx}{dt} = a^2\sqrt{1-e^2}(1-e\cos E)\frac{dE}{dt}, \tag{A19}$$

$$R^2\frac{dF}{dt} = X\frac{dY}{dt} - Y\frac{dX}{dt} = a^2\sqrt{1-e^2}(1+e\cos E)\frac{dE}{dt}. \tag{A20}$$

We note that up to this point, all the expressions referred to the primary and secondary foci have been reciprocal, in the sense that the former transform into the latter by exchanging the combination (r, f, e) with $(R, F, -e)$. This is simply a consequence of the symmetry of the ellipse (see Fig. 3 again).

It is well known that the time derivative of E is obtained by differentiating the Kepler equation as

$$\frac{dE}{dt} = \frac{n}{1-e\cos E}, \tag{A21}$$

where $n \equiv dM/dt$ is the mean motion. Thus the equations of motion for f and F can be expressed as

$$\frac{df}{dt} = \frac{na^2\sqrt{1-e^2}}{r^2} = \nu(1+e\cos f)^2, \tag{A22}$$

$$\frac{dF}{dt} = \left(\frac{na^2\sqrt{1-e^2}}{R^2}\right)\left(\frac{1+e\cos E}{1-e\cos E}\right)$$
$$= \nu\left(\frac{1-2e\cos F+e^2\cos^2 F}{1-2e\cos F+e^2}\right), \tag{A23}$$

where

$$\nu \equiv \frac{n}{(\sqrt{1-e^2})^3}. \tag{A24}$$

By means of the radius expressions and the magnitude of the orbital angular momentum,

$$L \equiv na^2\sqrt{1-e^2}, \tag{A25}$$

these are simply rewritten as

$$\frac{df}{dt} = \frac{L}{r^2}, \quad \frac{dF}{dt} = \frac{L}{rR}, \tag{A26}$$

the first of which is nothing but Kepler's second law of planetary motion.

APPENDIX B

SIMPLIFIED LINEAR TRANSFORMATION METHOD USING POSITION VECTOR

Let us summarize the first simplification of the linear transformation method provided in Paper V, that using the set of nine variables $(\boldsymbol{x}, \Delta\boldsymbol{L}, \Delta\boldsymbol{P})$.

Consider the perturbed two-body problem. Usually we adopt the pair of the relative position vector and the relative velocity vector referred to the heavier body, $(\boldsymbol{x}, \boldsymbol{v})$, as the basic set of variables to be integrated. Their equations of motion are

$$\frac{d\boldsymbol{x}}{dt} = \boldsymbol{v}, \quad \frac{d\boldsymbol{v}}{dt} = -\left(\frac{\mu}{r^3}\right)\boldsymbol{x} + \boldsymbol{a}. \tag{B1}$$

Here $\mu \equiv GM$ is the gravitational constant of the two-body problem, $r \equiv |\boldsymbol{x}|$ is the mutual distance between the two bodies, and $\boldsymbol{a}$ is the perturbing acceleration in the relative sense, which is expressed as a function of $\boldsymbol{x}$, $\boldsymbol{v}$, and the time t in general as

$$\boldsymbol{a} = \boldsymbol{a}(\boldsymbol{x}, \boldsymbol{v}, t). \tag{B2}$$

The conversion to the new set of variables from the ordinary set is as follows:

$$\Delta\boldsymbol{L} = \boldsymbol{L} - \boldsymbol{L}_0, \quad \Delta\boldsymbol{P} = \boldsymbol{P} - \boldsymbol{P}_0, \tag{B3}$$

where

$$\boldsymbol{L} = \boldsymbol{x}\times\boldsymbol{v}, \quad \boldsymbol{P} = \boldsymbol{v}\times\boldsymbol{L} - \mu\boldsymbol{n}, \quad \boldsymbol{n} = \boldsymbol{x}/r, \tag{B4}$$

and the quantities with the subscript zero are their initial values.

On the other hand, the reverse transformation is

$$\boldsymbol{v} = \frac{\boldsymbol{L}\times(\mu\boldsymbol{n}+\boldsymbol{P})}{L^2}, \tag{B5}$$

where $\boldsymbol{n}$, $\boldsymbol{L}$, and $\boldsymbol{P}$ are obtained as

$$\boldsymbol{n} = \boldsymbol{x}/r, \quad \boldsymbol{L} = \boldsymbol{L}_0 + \Delta\boldsymbol{L}, \quad \boldsymbol{P} = \boldsymbol{P}_0 + \Delta\boldsymbol{P}. \tag{B6}$$

The equations for the time development of the new variables are

$$\frac{d\boldsymbol{x}}{dt} = \boldsymbol{v}, \quad \frac{d\,\Delta\boldsymbol{L}}{dt} = \boldsymbol{M}, \quad \frac{d\,\Delta\boldsymbol{P}}{dt} = \boldsymbol{Q}, \tag{B7}$$

where

$$\boldsymbol{M} = \boldsymbol{x}\times\boldsymbol{a}, \quad \boldsymbol{Q} = \boldsymbol{a}\times\boldsymbol{L} + \boldsymbol{v}\times\boldsymbol{M}, \tag{B8}$$

and the velocity $\boldsymbol{v}$, the orbital angular momentum $\boldsymbol{L}$, and the perturbing acceleration $\boldsymbol{a}$ are evaluated from equations (B5), (B6), and (B2), respectively.

At each integration step, we modify the integrated position vector so as to satisfy the orthogonality relation with the angular momentum vector,

$$\boldsymbol{x}\cdot\boldsymbol{L} = 0, \tag{B9}$$

and the radius vector expression[16]

$$r = \frac{L^2}{\mu + \boldsymbol{P}\cdot\boldsymbol{n}}. \tag{B10}$$

This is done by means of two procedures. The first is an orthogonalization

$$\boldsymbol{x}' = \boldsymbol{x} - \left(\frac{\boldsymbol{L}\cdot\boldsymbol{x}}{L^2}\right)\boldsymbol{L}, \tag{B11}$$

[16] This is essentially the same as eq. (A4).

where the primed position is an intermediate quantity. The second is a scaling of the intermediate position,

$$\boldsymbol{x}^* = \left(\frac{L^2}{\mu r' + \boldsymbol{P}\cdot\boldsymbol{x}'}\right)\boldsymbol{x}', \tag{B12}$$

where $r' \equiv |\boldsymbol{x}'|$ and the position with an asterisk is the final position, to be used in the next step of the integration.

APPENDIX C

SIMPLIFIED LINEAR TRANSFORMATION METHOD USING ANTIFOCAL POSITION VECTOR

We next summarize a variation on the first simplification of the linear transformation method provided in Paper V that replaces the variable set with ($\boldsymbol{X}$, $\Delta\boldsymbol{L}$, $\Delta\boldsymbol{P}$). The conversion to the new set of variables from the ordinary set ($\boldsymbol{x}$, $\boldsymbol{v}$) is

$$\boldsymbol{X} = \boldsymbol{x} + \boldsymbol{S}, \quad \Delta\boldsymbol{L} = \boldsymbol{L} - \boldsymbol{L}_0, \quad \Delta\boldsymbol{P} = \boldsymbol{P} - \boldsymbol{P}_0, \tag{C1}$$

where the quantities needed are evaluated as follows:

$$\boldsymbol{L} = \boldsymbol{x}\times\boldsymbol{v}, \quad \boldsymbol{n} = \boldsymbol{x}/r, \quad \boldsymbol{P} = \boldsymbol{v}\times\boldsymbol{L} - \mu\boldsymbol{n}, \quad L^2 = \boldsymbol{L}\cdot\boldsymbol{L},$$
$$P^2 = \boldsymbol{P}\cdot\boldsymbol{P}, \quad \alpha = \frac{2L^2}{\mu^2 - P^2}, \quad \boldsymbol{S} = \alpha\boldsymbol{P}. \tag{C2}$$

The quantities with the subscript zero are initial values.

On the other hand, the reverse transformation is

$$\boldsymbol{x} = \boldsymbol{X} - \boldsymbol{S}, \quad \boldsymbol{v} = \frac{R\boldsymbol{L}\times(\mu\boldsymbol{N} - \boldsymbol{P})}{rL^2}, \tag{C3}$$

where the quantities needed are evaluated as

$$\boldsymbol{L} = \boldsymbol{L}_0 + \Delta\boldsymbol{L}, \quad \boldsymbol{P} = \boldsymbol{P}_0 + \Delta\boldsymbol{P}, \quad L^2 = \boldsymbol{L}\cdot\boldsymbol{L},$$
$$P^2 = \boldsymbol{P}\cdot\boldsymbol{P}, \quad \alpha = \frac{2L^2}{\mu^2 - P^2}, \quad \boldsymbol{S} = \alpha\boldsymbol{P}, \quad R^2 = \boldsymbol{X}\cdot\boldsymbol{X},$$
$$R = \sqrt{R^2}, \quad r = \mu\alpha - R, \quad \boldsymbol{N} = \boldsymbol{X}/R. \tag{C4}$$

The time development of the new variables is described by

$$\frac{d\boldsymbol{X}}{dt} = \boldsymbol{v} + \boldsymbol{U}, \quad \frac{d\,\Delta\boldsymbol{L}}{dt} = \boldsymbol{M}, \quad \frac{d\,\Delta\boldsymbol{P}}{dt} = \boldsymbol{Q}, \tag{C5}$$

where

$$\boldsymbol{M} = \boldsymbol{x}\times\boldsymbol{a}, \quad \boldsymbol{Q} = \boldsymbol{a}\times\boldsymbol{L} + \boldsymbol{v}\times\boldsymbol{M}, \quad \boldsymbol{U} = \beta\boldsymbol{P} + \alpha\boldsymbol{Q},$$
$$\beta \equiv \frac{d\alpha}{dt} = \frac{2\alpha(\boldsymbol{L}\cdot\boldsymbol{M}) + \alpha^2(\boldsymbol{P}\cdot\boldsymbol{Q})}{L^2}, \tag{C6}$$

and the quantities $\boldsymbol{x}$, $\boldsymbol{v}$, $\boldsymbol{L}$, $\boldsymbol{P}$, and α are obtained during the reverse transformation.

At each integration step, we modify the integrated antifocal position vector so as to satisfy the orthogonality relation[17] with the angular momentum vector,

$$\boldsymbol{X}\cdot\boldsymbol{L} = 0, \tag{C7}$$

and the condition

$$R = \frac{L^2}{\mu - \boldsymbol{P}\cdot\boldsymbol{N}}, \tag{C8}$$

which is essentially the same as equation (A3). This is again done by means of two procedures. The first is the orthogonalization

$$\boldsymbol{X}' = \boldsymbol{X} - \left(\frac{\boldsymbol{L}\cdot\boldsymbol{X}}{L^2}\right)\boldsymbol{L}, \tag{C9}$$

where the primed position is an intermediate quantity. The second is a scaling of the intermediate position,

$$\boldsymbol{X}^* = \left(\frac{L^2}{\mu R' - \boldsymbol{P}\cdot\boldsymbol{X}'}\right)\boldsymbol{X}', \tag{C10}$$

where $R' \equiv |\boldsymbol{X}'|$ and the position with an asterisk is the final position to be used in the next step of integration.

APPENDIX D

ANTIFOCAL ORBITAL LONGITUDE METHOD

Finally, we summarize the variation of the true-longitude method presented in Paper VI that replaces the true orbital longitude with the antifocal one, w. The resulting new method uses the set of variables (w, $\Delta\boldsymbol{L}$, ΔP_A, ΔP_B).

The conversion to the new set of variables from the ordinary set ($\boldsymbol{x}$, $\boldsymbol{v}$) is

$$w = \tan^{-1}(N_B/N_A), \quad \Delta\boldsymbol{L} = \boldsymbol{L} - \boldsymbol{L}_0,$$
$$\Delta P_A = P_A - (P_A)_0, \quad \Delta P_B = P_B - (P_B)_0, \tag{D1}$$

where the quantities with subscript zero are initial values. The quantities needed here are evaluated as follows:

$$r^2 = \boldsymbol{x}\cdot\boldsymbol{x}, \quad r = \sqrt{r^2}, \quad \boldsymbol{n} = \boldsymbol{x}/r, \quad \boldsymbol{L} = \boldsymbol{x}\times\boldsymbol{v},$$
$$\boldsymbol{P} = \boldsymbol{v}\times\boldsymbol{L} - \mu\boldsymbol{n}, \quad L^2 = \boldsymbol{L}\cdot\boldsymbol{L}, \quad P^2 = \boldsymbol{P}\cdot\boldsymbol{P},$$
$$\alpha = \frac{2L^2}{\mu^2 - P^2}, \quad \boldsymbol{S} = \alpha\boldsymbol{P}, \quad \boldsymbol{X} = \boldsymbol{x} + \boldsymbol{S}, \quad R^2 = \boldsymbol{X}\cdot\boldsymbol{X},$$
$$R = \sqrt{R^2}, \quad \boldsymbol{N} = \boldsymbol{X}/R, \quad L = \sqrt{L^2}, \quad \boldsymbol{e}_C = \boldsymbol{L}/L,$$
$$\boldsymbol{A} = \boldsymbol{B}_0\times\boldsymbol{L}, \quad A^2 = \boldsymbol{A}\cdot\boldsymbol{A}, \quad A = \sqrt{A^2}, \quad \boldsymbol{e}_A = \boldsymbol{A}/A,$$
$$\boldsymbol{e}_B = \boldsymbol{e}_C\times\boldsymbol{e}_A, \quad N_A = \boldsymbol{N}\cdot\boldsymbol{e}_A, \quad N_B = \boldsymbol{N}\cdot\boldsymbol{e}_B,$$
$$P_A = \boldsymbol{P}\cdot\boldsymbol{e}_A, \quad P_B = \boldsymbol{P}\cdot\boldsymbol{e}_B. \tag{D2}$$

Here

$$\boldsymbol{B}_0 \equiv \boldsymbol{L}_0\times\boldsymbol{x}_0 \tag{D3}$$

must be computed in advance. Note that the condition $|w| < \pi$ holds.

On the other hand, the reverse transformation is

$$\boldsymbol{x} = x_A\boldsymbol{e}_A + x_B\boldsymbol{e}_B, \quad \boldsymbol{v} = v_A\boldsymbol{e}_A + v_B\boldsymbol{e}_B, \tag{D4}$$

[17] This is valid because another orthogonality relation, $\boldsymbol{L}\cdot\boldsymbol{P} = 0$, holds even under perturbations.

where the quantities needed are evaluated as

$$N_A = \cos w, \quad N_B = \sin w, \quad P_A = (P_A)_0 + \Delta P_A,$$
$$P_B = (P_B)_0 + \Delta P_B, \quad L^2 = \boldsymbol{L}\cdot\boldsymbol{L}, \quad P^2 = (P_A)^2 + (P_B)^2,$$
$$R = \frac{L^2}{\mu - (P_A N_A + P_B N_B)}, \quad \alpha = \frac{2L^2}{\mu^2 - P^2},$$
$$r = \mu\alpha - R, \quad L = \sqrt{L^2}, \quad \gamma = R/(rL),$$
$$x_A = RN_A - \alpha P_A, \quad x_B = RN_B - \alpha P_B,$$
$$v_A = \gamma(-\mu N_B + P_B), \quad v_B = \gamma(\mu N_A - P_A). \tag{D5}$$

In evaluating N_A and N_B in the above, we recommend use of our fast procedure given in Paper VI to evaluate the sine and cosine functions simultaneously. The expressions for $\boldsymbol{x}$, $\boldsymbol{v}$, and $\boldsymbol{P}$ in terms of A- and B-components automatically satisfy the conditions of orthogonality with the orbital angular momentum, $\boldsymbol{x}\cdot\boldsymbol{L} = \boldsymbol{v}\cdot\boldsymbol{L} = \boldsymbol{P}\cdot\boldsymbol{L} = 0$, which significantly contributes to the reduction of integration errors.

The equations for the time development of the new variables are

$$\frac{dw}{dt} = \Omega_W + \Omega_S + \Omega_F, \quad \frac{d\,\Delta\boldsymbol{L}}{dt} = \boldsymbol{M},$$
$$\frac{d\,\Delta P_A}{dt} = Q_A - \Omega_F P_B, \quad \frac{d\,\Delta P_B}{dt} = Q_B + \Omega_F P_A. \tag{D6}$$

The quantities needed in the above are evaluated as follows:

$$\boldsymbol{M} = \boldsymbol{x}\times\boldsymbol{a}, \quad \Omega_W = \frac{L}{rR}, \quad \Omega_F = \frac{(\boldsymbol{B}_0\times\boldsymbol{e}_B)\cdot\boldsymbol{M}}{A},$$
$$\boldsymbol{Q} = \boldsymbol{a}\times\boldsymbol{L} + \boldsymbol{v}\times\boldsymbol{M}, \quad Q_A = \boldsymbol{Q}\cdot\boldsymbol{e}_A, \quad Q_B = \boldsymbol{Q}\cdot\boldsymbol{e}_B,$$
$$\beta = \frac{2\alpha(\boldsymbol{L}\cdot\boldsymbol{M}) + \alpha^2(P_A Q_A + P_B Q_B)}{L^2},$$
$$U_A = \beta P_A + \alpha Q_A, \quad U_B = \beta P_B + \alpha Q_B,$$
$$\Omega_S = \frac{N_A U_B - N_B U_A}{R}, \tag{D7}$$

where the quantities not explicitly written here are evaluated in the process of the reverse transformation, equation (D5).

At each integration step, we perform the domain reduction of w as

```
if (w > π) {w -= 2π;} else if (w < -π) {w += 2π;} ;
```

Then the condition $|w| < \pi$ is always satisfied throughout the integration.

REFERENCES

Fukushima, T. 2003a, AJ, 126, 1097 (Paper I)
———. 2003b, AJ, 126, 2567 (Paper II)
———. 2003c, AJ, 126, 3138 (Paper III)
———. 2004a, AJ, 127, 3638 (Paper IV)
Fukushima, T. 2004b, AJ, 128, 920 (Paper V)
———. 2004c, AJ, 128, 1446 (Paper VI)
———. 2004d, Celest. Mech. Dyn. Astron., submitted (Paper VII)